Green Chemistry

PAPER

View Article Online
View Journal | View Issue

Cite this: *Green Chem.*, 2022, **24**, 2975

Distinct cellulose nanofibrils generated for improved Pickering emulsions and lignocellulose-degradation enzyme secretion coupled with high bioethanol production in natural rice mutants†

Hao Peng,‡[a,b] Wenyue Zhao,‡[a] Jingyuan Liu,[a,b] Peng Liu,[a,b] Haizhong Yu,[b] Jun Deng,[a] Qiaomei Yang,[a,b] Ran Zhang,[a,b] Zhen Hu,[a,b] Shilin Liu,[c] Dan Sun,[d] Liangcai Peng[a,b] and Yanting Wang *[a,b]

Since lignocellulose represents an enormous and sustainable biomass resource convertible for biofuels and bioproducts, green-like and cost-effective technology is being increasingly considered to generate value-added bioproducts along with biofuel production. Herein, we took advantage of the natural rice mutant (*Osfc16*) that possesses recalcitrance-reduced lignocellulose, and performed a direct enzymatic hydrolysis of rice straw to achieve significantly increased bioethanol yields (by 19% at $p < 0.01$) compared with those from the wild type. Additionally, we generated optimal cellulose nanofibrils (CNFs) from the remaining enzymatic residues under far fewer cycles of high-pressure homogenization. Notably, due to their characteristic surfaces, the CNFs at low dosage not only act as effective inducers for the secretion of cellulase complexes by *T. reesei*, with protein yields significantly increased by 99% and enzyme (endoglucanases and xylanases) activities by 27% and 51%, respectively, using full rice straw as the carbon source, but also play a more efficient role as stabilizers for improving almost all major parameters of Pickering emulsions, including the emulsion index, droplet size, interfacial tension, zeta potential, water holding capacity and storage condition, compared to other chemical inducers and stabilizers (CNFs, proteins, and starch) that have been applied in previous studies. Hence, this study proposes a mechanistic model to elucidate why the desirable rice mutant enables the generation of distinct CNFs that are favorable for Pickering emulsion stabilization and mixed-cellulase induction coupled with relatively low-cost bioethanol production, providing multiple non-chemical processes as a novel green-like technology for complete biomass utilization towards the production of low-cost bioethanol and high-value bioproducts.

Received 29th November 2021,
Accepted 2nd March 2022

DOI: 10.1039/d1gc04447h

rsc.li/greenchem

1. Introduction

As the most abundant biomass on Earth, lignocellulose is sustainable and can be converted into biofuels and other bioproducts.[1,2] However, lignocellulose recalcitrance has become a critical issue restricting biomass enzymatic saccharification, and thus requires loading large amounts of high-cost lignocellulose-degradation enzymes.[3,4] To address this recalcitrance, genetic modifications of plant cell walls have been implemented in bioenergy crops for a green-like and cost-effective biomass process.[5] In particular, in terms of cellulose as a major wall component, its features, such as the cellulose crystalline index (CrI) and degree of polymerization (DP), have been recently improved in genetic mutants and transgenic lines, leading to near-complete biomass enzymatic hydrolysis and maximum bioethanol production.[6,7] Although cellulosic ethanol has been regarded as a perfect additive in petrol fuels, there remains a technical difficulty in achieving economic

[a]*Biomass & Bioenergy Research Center, College of Plant Science & Technology, Huazhong Agricultural University, Wuhan 430070, China. E-mail: wyt@mail.hzau.edu.cn; Fax: +86-27-87280016; Tel: +86-27-87281765https://bbrc.hzau.edu.cn*

[b]*Laboratory of Biomass Engineering & Nanomaterial Application in Automobiles, College of Food Science & Chemical Engineering, Hubei University of Arts & Science, Xiangyang, China*

[c]*College of Food Science& Technology, Huazhong Agricultural University, Wuhan 430070, China*

[d]*Hubei Provincial Key Laboratory of Green Materials for Light Industry, Collaborative Innovation Center of Green Light-Weight Materials & Processing, Hubei University of Technology, Wuhan 430068, China*

†Electronic supplementary information (ESI) available. See DOI: 10.1039/d1gc04447h

‡Equal contributor.

benefits from large-scale biomass processes due to the low energy density of lignocellulose.[8] Alternatively, it is being increasingly considered to investigate highly valued bioproducts and byproducts from lignocellulose residues.[9,10]

Pickering emulsions, a type of emulsion that uses solid particles to stabilize the oil–water interface, show relatively high resistance to droplet coalescence.[11] Moreover, the solid particles are applicable for food emulsions, as most of them are derived from proteins, lipids and starch.[12] To generate new food-grade Pickering emulsions, recent attempts have explored cellulosic biomass, as cellulose can strongly form a steric barrier during the emulsion formation to protect the droplets from flocculation or coalescence.[13,14] For instance, highly stable O/W Pickering emulsions have been achieved using cellulose nanofibrils from *Miscanthus* straws.[15] Mechanical pretreatment, especially high-pressure homogenization, is considered a relatively simple and green-like method.[16,17] In addition, the CNFs obtained from homogenization are of relatively high nanosized fraction, transparency degree and stability, compared to other methods.[18] However, it remains to explore fine cellulose nanofibrils for further improved Pickering emulsions, and it also needs to test its novel enhancements on biomass enzymatic saccharification and cellulase enzyme production.

As a commonly applicable microorganism, *Trichoderma reesei* strain has been used to secret biomass-degrading enzyme complexes including four major types of enzymes: exoglucanases (CBH), endoglucanases (EG), β-glucosidases (BG) and xylanases, which could act together for complete lignocellulose hydrolysis.[19,20] In principle, endoglucanases first cleave cellulose microfibers to release small cellulose fragments, which are then acted upon by exoglucanases to produce oligosaccharides and cellobiose, and finally, β-glucosidases convert them into glucose *via* hydrolysis.[21,22] In addition, the β-1,4-glycosidic backbone of xylan is cleaved by xylanase, an essential group of hydrolytic enzyme, and its enzymatic products are xylose, xylobiose and xylooligosaccharides.[23] However, as lignocellulose residues have complicated structures and diverse compositions, lignocellulose degradation basically requires large amounts of cellulases and xylanases at optimal proportions.[24] Cellulases, the most significant and integral part of biochemical conversion from lignocellulosic residues, have been regarded as one of the crucial factors for sustainable and large-scale bioethanol production.[25] Although the cost of cellulases has been reduced over the past years, there are still challenges for further improvement in cellulase production.[26–30] In particular, both enzyme yield and activity limit to reduce the efficiency of cellulases.[31] Therefore, it is very important to find out the low-cost and high-efficiency lignocellulose substrates that enable inducing *T. reesei* for optimal secretion of cellulases and xylanases.[32]

Rice is a major food crop over the world with enormous lignocellulose-rich residues. In our previous studies, a natural rice mutant (*Osfc16*) defective at cellulose biosynthesis has been examined with significantly lessened lignocellulose recalcitrance such as reduced cellulose CrI and DP values.[33] In this study, we initially used this desirable rice mutant to generate distinct cellulose nanofibrils (CNFs) from its raw straws and the residues after biomass enzymatic saccharification by performing optimal homogenization at a high pressure. We then examined that the CNFs of rice mutants could act as excellent stabilizers for significantly improved Pickering emulsions, compared to rice wild type (WT). Notably, this study found out that the CNFs, which were obtained from direct enzymatic saccharification of rice mutant straws, could remarkably induce the *T. reesei* strain to secret cellulases and xylanases in high yields and activity, providing an integrated strategy for complete biomass utilization for low-cost bioethanol production and high-value bioproducts.

2. Materials and methods

2.1. Biomass sample collection and commercial enzyme purchase

The biomass samples of rice mutants (*Osfc16*) and wild types (WT; Nipponbare) were collected from the experimental fields of Huazhong Agricultural University. The mature stem tissues were dried at 55 °C, cut into small pieces, ground through 40-mesh screen and stored in a dry container. The mixed-cellulase enzymes of HSB were purchased from Imperial Jade Biotechnology Co., Ltd, Ningxia, China.

2.2. Cellulose nanofibril (CNF) extraction

The ground biomass powders (10 g) were incubated with 5% NaOH at 60 °C for 1 h for 5 times and then treated with 0.5% NaClO at 60 °C for 1 h for 3 times.[34] The solid residues were filtered, washed with distilled water to neutral, and disintegrated using a high-speed blender (Ultra Turrax T18, IKA, Germany) at 11 000 rpm for 5 min at room temperature. The suspension was further homogenized at 60 MPa using a high-pressure homogenizer (HPH) (AH-1500, ATS, Canada) for various cycle times to achieve CNF samples, which are termed HPH-5t, HPH-10t, HPH-20t and HPH-30t corresponding to the homogenized cycles of 5, 10, 20, and 30 times, respectively.

2.3. Pickering emulsion preparation

Coarse oil-in-water emulsions were initially prepared by mixing 10% dodecane and 90% water (90 v%) with 0.1% CNF samples as described previously.[15] The samples of Pickering emulsions were placed at different storage temperatures (4 °C, 25 °C, and 50 °C), pH values (3, 5, and 7) and storage periods (3 d, 7 d, 14 d, and 28 d). All experiments were performed independently in triplicate.

2.4. Pickering emulsion characterization

Pickering emulsions were characterized by evaluating the emulsion index (EI%) and droplet size as described previously.[35] EI was calculated using the following formula:

$$\mathrm{EI}\ (\%) = H_c/H_t \times 100\%,$$

where H_c is the height of the cream layer and H_t is the total height of the emulsions.

The droplet polydispersity was measured using a MasterSizer 2000 (Malvern Instruments, Worcestershire, UK). The droplet polydispersity is expressed as the surface-weighted mean diameter:[36]

$$d_{3,2} = \sum_i n_i d_i^3 / \sum_i n_i d_i^2,$$

where n_i is the number of droplets of diameter d_i.

The interfacial tension of CNFs (0.01%) samples was tested using a drop shape analyzer rheometer (Tracker Teclis/IT Concept, France) at 25 °C. The aqueous phase was placed in an optical glass cuvette, and a syringe filled with dodecane as the oil phase was then submerged into the optical glass cuvette. During the whole experiment, the initial volume of the oil drop was all to 10 μL. Distilled water was used as the control. The surface charge of the CNFs was determined using a dynamic light scattering/electrophoresis instrument (Zetasizer Nano ZS, Malvern Instruments, Worcestershire, UK). The water holding capacity (WHC) of CNFs with different physical sizes was measured, and it was calculated using the following formula:[37]

$$\text{WHC } (\%) = (M_{\text{wet}} - M_{\text{dry}})/M_{\text{dry}} \times 100\%,$$

where M_{wet} is the wet weight of the CNFs and M_{dry} is the dry weight of CNFs.

The rheological properties of the emulsions were characterized using a Discovery HR-2 Hybrid Rheometer (TA Instruments, New Castle, DE, USA) with concentric cylinder geometry. The temperature was set to 25.0 ± 0.1 °C. A dynamic frequency sweep was carried out by applying a constant strain of 0.65% (selected by measuring the linear domain), and the storage modulus (G') and loss modulus (G'') as a function of frequency were obtained. The range of shear rate was 0.01–10 s^{-1} and the frequency was 0.1–100 rad s^{-1}. All analyses were performed independently in triplicate.

2.5. Cellulose nanofibril (CNF) observation

Atomic force microscopy (MultiMode8, Bruker, USA) was applied to observe the topography of CNFs.[13] The samples were diluted to 0.01% with distilled water and the test was performed at a scan rate of 1 Hz. The average defect distances of AFM general images were measured using the Gwyddion software.

2.6. Enzymatic hydrolysis and yeast fermentation

The powders of raw rice straws were washed once with 0.2 M phosphate buffer (pH 4.8), and incubated with 3.2 g L^{-1} mixed-cellulase enzymes (HSB) with final concentrations of cellulases at 1.6 g L^{-1} for 48 h at 50 °C, while co-supplied with 1% (v/v) Tween-80. The yeast fermentation was conducted using *Saccharomyces cerevisiae* strain (Angel Yeast Co., Ltd, Yichang, China) and the ethanol yield was estimated by the $K_2Cr_2O_7$ method, as described previously.[38–40] Absolute ethanol (99.9%) was used as the standard. All experiments were performed in technological triplicate.

2.7. *T. reesei* strain cultivation co-supplied with rice CNFs

T. reesei strain (Rut-C30 and CICC 40348) was obtained from the China Center of Industrial Culture Collection. The strain was grown on potato dextrose agar at 30 °C for 7 d and 5d for two batch of experiments, and the flask cultivations conidia were harvested with ddH_2O and counted using a haemocytometer. The spore germination rates were accurately examined for appropriate incubation time prior to micro fluidic analysis and sorting. The spores were collected and adjusted to a density of 6×10^6 spores per mL in a liquid cellulase-inducing medium, and 500 μL of spore suspension was then incubated under 200 rpm min^{-1} shaking at 30 °C for 7 d. The Mandels–Andreotti medium was applied as described previously,[41] and the pH value was adjusted to 4.8. The liquid culture was added with rice straw substrates as a carbon source co-supplied with low dosage of rice CNFs to induce cellulase production from *T. reesei.* Another liquid culture was only added with low dosage of rice CNFs to induce cellulases. All experiments were performed independently in triplicates.

2.8. Filter paper activity (FPA) detection and SDS-PAGE running

The FPA and protein content of crude cellulase solutions secreted by *T. reesei* were estimated, as described previously.[41] About 1 mL crude cellulase solution secreted by *T. reesei* was mixed with 3 mL 0.05 M citrate buffer (pH 4.8) and then loaded into a test tube with 50 mg Whatman filter paper (No. 1 grade). The reaction mixture was incubated for 60 min at 50 °C and the reaction was terminated by adding 2 mL DNS, followed by the addition of boiling water for 10 min. One FPA unit was defined by measuring the amount of enzyme releasing 1 mmol reducing sugar per min from the Whatman filter paper. The protein content of the crude cellulase solution was determined by a Coomassie Brilliant Blue G250 dye assay, as described previously.[41] The absorbance of the protein–dye complex was read at 595 nm using a UV-vis spectrometer (V-1100D, Shanghai MAPADA Instruments Co., Ltd, Shanghai).[42] SDS-PAGE was conducted using Stain-Free precast gels (Beijing Zoman Biotechnology Co., Ltd), as described previously.[41] About 30 mL crude cellulase solution was loaded into each well. Proteins of SDS gel were visualized with colloidal Coomassie blue staining.

2.9. Endoglucanase, exoglucanase, β-glucosidase and xylanase activity assay *in vitro*

All enzyme activity assays were performed *in vitro*, as described previously.[41,43] Endoglucanase, exoglucanase, β-glucosidase and xylanase activities were respectively measured using carboxymethylcellulose (CMC-Na), pNPC, salicin and beechwood xylan as substrates (purchased from China National Pharmaceutical Group Co., Ltd, Shanghai Yuanye Bio-Technology Co., Ltd, China). The endoglucanase activity was determined in the reaction mixture containing 0.5 mL of suitable diluted enzyme and 1 mL of 1% (w/v) CMC-Na solution in 0.05 M sodium citrate buffer (pH 4.8) at 50 °C for 30 min.

Exoglucanase, β-glucosidase and xylanase activities were measured under the same conditions, except that CMC-Na was replaced with 0.25 mL of 1 mg mL^{-1} pNPC, 1 mL 1% salicin and 1.5 mL 1% xylan solution. The reducing sugars released were determined by a dinitrosalicylic acid (DNS) method except exoglucanases. About 2 mL DNS was added to stop the reaction by treating at 100 °C for 5 min. Once the reaction solution was cooled to room temperature, the absorbance was read at 540 nm. For exoglucanase assay, about 0.75 mL 10% Na_2CO_3 was added to stop the reaction and the absorbance was read at 420 nm. All assays were performed independently in triplicate.

2.10. Lignocellulose residue characterization

The CrI of lignocellulose samples was detected by X-ray diffraction (XRD) (Rigaku-D/MAX instrument, Ultima III, Japan), as described previously.[44] The lignocellulose residues obtained from *T. reesei* induction were applied under plateau conditions, and the CrI was calculated using the intensity of the 200 peak (I_{200}, θ = 22.5°) and the intensity at the minimum between the 200 and 110 peaks (I_{am}, θ = 18.5°) as follows: CrI = $(I_{200} - I_{am}) \times 100/I_{200}$. I_{200} represents both the crystalline and amorphous materials, while I_{am} represents the amorphous material. Technical standard errors of the CrI method were detected at ±0.05–0.15 using five representative samples in triplicate. Fourier transform infrared (FT-IR) spectroscopy was applied to scan the lignocellulose residues using a FT-IR analyzer (470-Nexus, Nicolet, USA) in wavenumbers ranging from 400 to 4000 cm^{-1}, as described previously.[7]

2.11. Proteomic analysis

Total crude cellulases secreted by *T. reesei* were analyzed by LC-MS/MS (Jingjie PTM BioLab Co., Ltd, Hangzhou, China; Orbitrap Elite LC-MS/MS, Thermo, USA), as described previously.[41] About 200 mg proteins were rehydrated in 10 mM dithiothreitol and incubated at 37 °C for 60 min. The alkylation was performed using iodoacetamide for 45 min under darkness, and the samples were desalted and collected using a Microcon YM-10 Centrifugal Filter Unit. The obtained proteins were digested thoroughly using trypsin (a trypsin-protein ratio of 1 : 50, w/w) for 16 h. The resulting peptide mixtures were lyophilized after desalting with a ZipTip C18 column and then dissolved in double-distilled H_2O. The tryptic peptides were dissolved in 0.1% formic acid (solvent A) and directly loaded onto a home-made reversed-phase analytical column (1.8 mm, 0.15 × 1.00 mm). The gradient comprised an increase from 4% to 18% solvent B (0.1% formic acid in 100% acetonitrile) over 182 min, 18–90% in 5 min and holding at 90% for the last 8 min, and all were fixed at a constant flow rate of 300 nL min^{-1} using an EASY-nLC 1000 UPLC system. The peptides were subjected to NSI source followed by tandem mass spectrometry (MS/MS) in Thermo Fisher LTQ Orbitrap ETD coupled online to the UPLC. The electrospray voltage was 2.0 kV, the *m*/*z* scan range was 350–1600 for full scan, and intact peptides were detected in the Orbitrap at a resolution of 30 000. Peptides were then selected for MS/MS using NCE setting as 35 and the fragments were detected in the Orbitrap at a resolution of 17 500. A data-dependent procedure that alternated between one MS scan was followed by 20 MS/MS scans with 15.0 s dynamic exclusion. Automatic gain control (AGC) was set at 5E4. Liquid chromatography-MS/MS analysis data were identified by searching the *T. reesei* Rut-C30 protein sequence databases downloaded from Uniprot.

2.12. Statistical analysis

Statistical analysis was carried out using a Superior Performance Software System (SPSS version 16.0, Inc., Chicago, IL). Pair-wise comparisons were completed by Student's *t*-test. All measurements were carried out in independent triplicate with the average values calculated from the original triplicate measurements.

3. Results and discussion

3.1. Distinct cellulose nanofibrils of *Osfc16* mutants for significantly stabilizing Pickering emulsions

Using our previously identified rice mutant (*Osfc16*) that is of recalcitrance-reduced lignocellulose,[33] this study extracted the cellulose nanofibrils (CNFs) from either its mature raw straws or the residues obtained from direct enzymatic hydrolysis of raw straws (Fig. 1; Table S1†). By performing high-pressure homogenization (HPH) under different cycle times (5t, 10t, 20t, and 30t) for diverse CNF products termed HPH-5t, -10t, -20t and -30t, we prepared Pickering emulsions stabilized with 0.1% CNFs (Fig. 1A and B; Fig. S1†). As a result, the Pickering emulsions stabilized with the CNFs of *Osfc16* mutant were detected with significantly higher emulsion index (EI) values than those of the wild type (WT) by 4–18% at $p < 0.05$ or 0.01 level ($n = 3$) among the most CNF samples examined (Fig. 1C and D), suggesting that the emulsions prepared with the CNFs of *Osfc16* samples should be stabler against coalescence or phase separation. Furthermore, this work examined that HPH-5t and HPH-10t of enzymatic residues had higher EI values than those of raw straws in both *Osfc16* and WT. In addition, either HPH-20t of raw straws or HPH-10t of enzymatic residues were respectively of the highest EI values compared to other samples, indicating that the optimal CNFs from the enzymatic residues should require much less HPH cycle times than those from the raw straws.

3.2. Linear enhancements of Pickering emulsions by CNFs of *Osfc16* mutants

To test how the Pickering emulsions are improved by CNF stabilization in the *Osfc16* mutant samples, this study prepared Pickering emulsions by supplying a series of dosages of CNFs obtained from raw rice straws and enzymatic residues under optimal HPH cycle times (Fig. 2). In general, all four *Osfc16* mutant and WT samples showed a typically linear enhancement of EI values, as their CNF dosages were raising from 0.05% to 0.5%. In particular, no excess oil was visible on the top of the emulsions from 0.5% CNF supplement, indicating

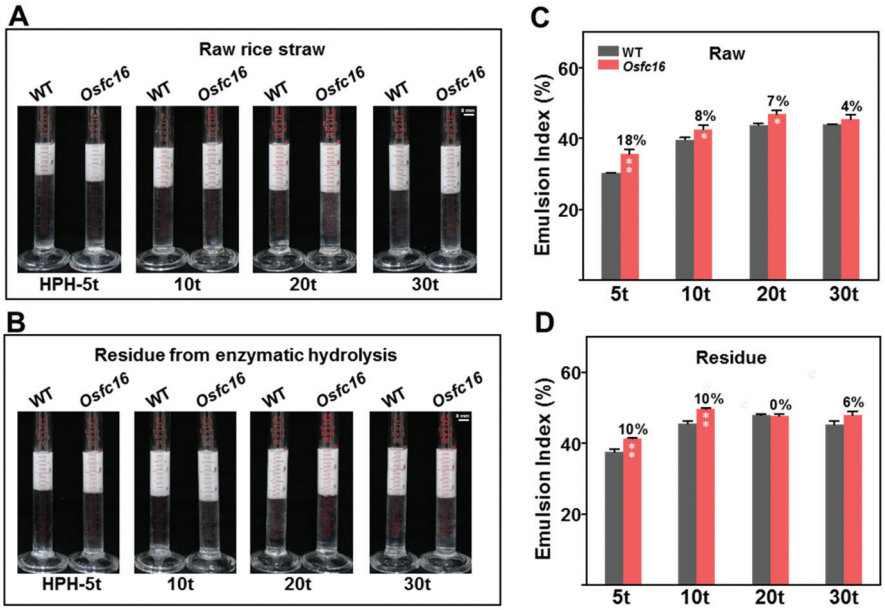

Fig. 1 Pickering emulsions stabilized with 0.1% CNFs generated under different cycles of high-pressure homogenization (HPH) in the *Osfc16* mutant and wild-type (WT) samples. (A and B) Images of Pickering emulsions prepared from rice straws and lignocellulose residues of the direct enzymatic hydrolysis of straws. (C and D) Emulsion index (EI) of all samples examined. All emulsion samples consist of oil and water in a 1 : 9 proportion. * and ** represent significant difference between the mutant and WT samples using the Student's *t*-test at the $p < 0.05$ and <0.01 levels ($n = 3$), respectively, with the increased percentage of the mutant relative to the WT, and the data are expressed as mean ± SD ($n = 3$).

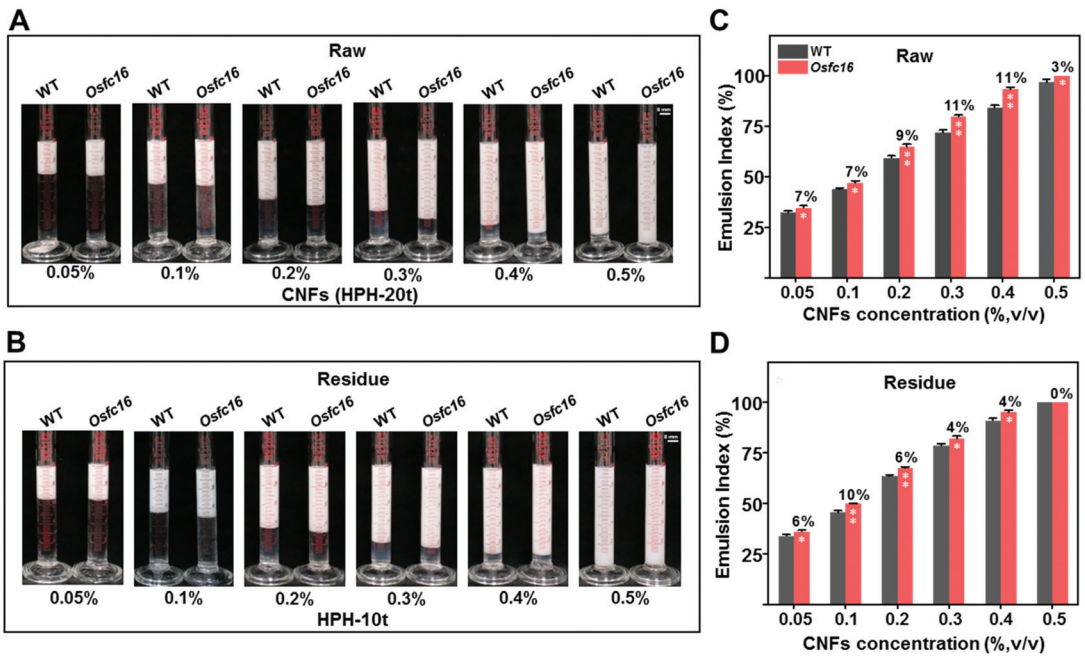

Fig. 2 Pickering emulsions stabilized with a series of dosages of CNFs generated from the *Osfc16* mutant and WT samples. (A and B) Images of Pickering emulsions prepared from rice straws and lignocellulose residues. (C and D) Emulsion index (EI) of all samples examined. All emulsion samples consist of oil and water in a 1 : 9 proportion. * and ** represent significant difference between the mutant and WT samples using the Student's *t*-test at the $p < 0.05$ and <0.01 levels ($n = 3$), respectively, with the increased percentage of the mutant relative to the WT, and the data are expressed as mean ± SD ($n = 3$).

that a permanent state of emulsion index should be reached. The results thus suggested that these CNFs at low dosages should have a significant impact on the formation of the 3D network system, probably due to the inhibition of the emulsion droplet from freely moving.[45,46] By comparison, two *Osfc16* mutant samples (raw straws, enzymatic residues) were

respectively of significantly higher EI values than those of the WT by 3–11% at $p < 0.05$ or 0.01 level ($n = 3$) in almost all samples examined except for the 0.5% residues, which confirmed that the *Osfc16* mutant could generate desirable CNFs for much more improved emulsion stability. Furthermore, all the samples exhibited significantly higher EI values at 100% with 0.5% CNF dosages than that of the CNF generated from starch.[12] Meanwhile, HPH-20t raw sample of *Osfc16* mutants retained a relatively increased EI value at 64.80% with 0.2% CNFs, whereas the *Miscanthus* CNFs showed an EI value at 52%, as described previously,[15] indicating an improved stability of Pickering emulsions with desirable CNFs.

3.3. Largely reduced droplet size and interfacial tension with increased water holding capacity of Pickering emulsions in *Osfc16* samples

As the optimal CNFs generated from *Osfc16* mutants could better stabilize Pickering emulsions described above, this study observed optical images of the Pickering emulsions with a typical unimodal distribution of droplet size (Fig. 3A and B). As a comparison, the emulsions of *Osfc16* mutant samples appeared to be more stable than those of the WT, due to its relatively small droplet size. Meanwhile, the emulsions of rice mutant samples were of obviously reduced dynamic interfacial tension at the oil–water interface, compared to the WT samples (Fig. 3C). As all four samples had much lower equilibrium values than the blank sample did, it suggested that the CNFs should be typically Pickering solid particle stabilizers for less relaxation (adsorption and rearrangement) time.[47] While the CNF homogenization cycle times were raising from 5t to 30t, their zeta potentials remained decreasing from −14 mV to −21 mV, and in particular two mutant samples (raw straws and enzymatic residues) had relatively low zeta values than those of the WT (Fig. 3D). As a result, all four samples showed a raising water holding capacity from HPH-5t to HPH-30t (Fig. 3E). Consistently, two mutant samples were respectively of much higher water holding capacities than those of the WT, and two enzymatic residues of the mutant and WT samples remained higher capacities than those of their raw straw samples. Hence, the results indicated that the CNFs prepared with the enzymatic residue of *Osfc16* mutant should be the optimal stabilizer for much improved Pickering emulsions, which could be applicable for a particle emulsifier in the food industry.[48]

In addition, as the CNFs were of a typically shear thinner fluid,[49] this study determined a decreasing viscosity for the increase in shear rate (Fig. S2†). However, it was quite easy to entangle with each other and to form a strong 3D network as the structure of nanofibrils. Hence, the declined viscosity of CNFs suggested that the interact network structure in CNFs was violently destroyed.[50] In addition, storage modulus was higher than its corresponding loss modulus, indicating the elastic behavior of particle-stabilized emulsions.[51]

3.4. Consistently improved stability of Pickering emulsions under different storage conditions in *Osfc16* samples

Since the stability of Pickering emulsions is a major factor affected by storage conditions,[52] this study detected any alteration of emulsifying property under different storage temperatures and pH values (Fig. 4). Using the Pickering emulsions

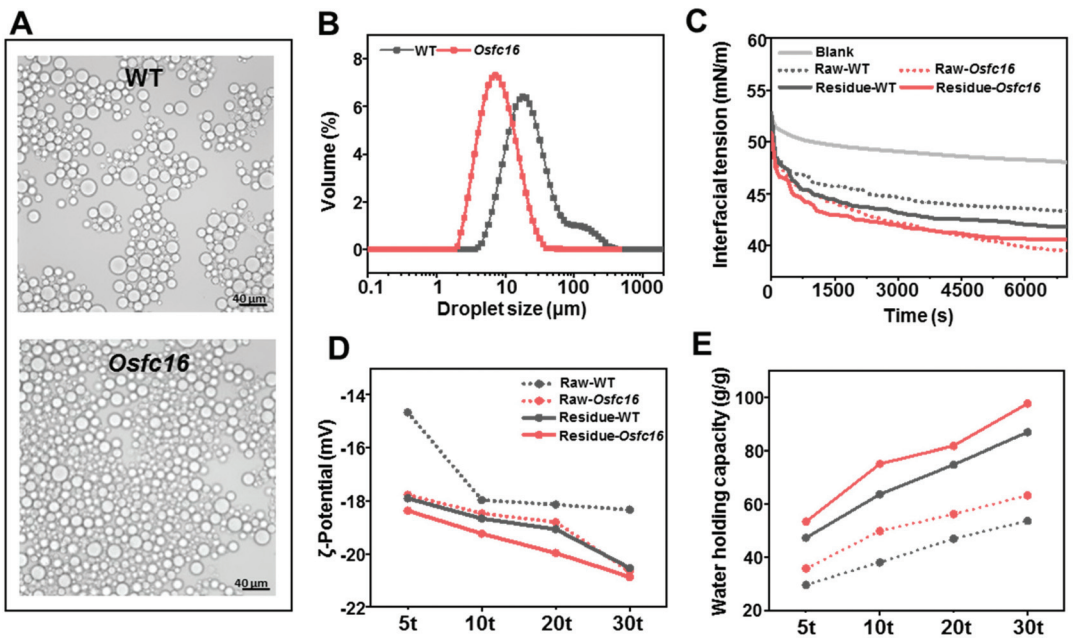

Fig. 3 Analyses of major parameters of Pickering emulsions stabilized with CNFs generated from *Osfc16* and WT samples. (A and B) Optical microscopy images and particle size distribution of the Pickering emulsions with 0.1% CNFs of enzymatic residues. (C) Dynamic interfacial tension at the oil–water interface as a function of time with 0.01% CNFs. CNFs from HPH-20t of raw rice straws or HPH-10t of enzymatic residue. (D and E) Zeta potential and water holding capacity of the 0.1% CNFs from HPH-10t.

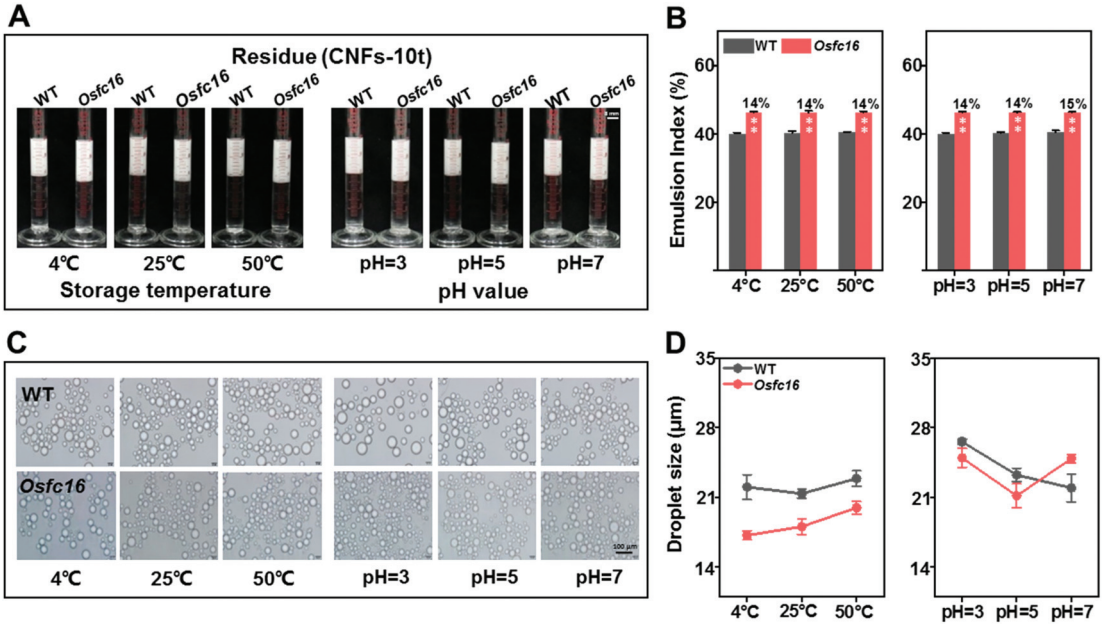

Fig. 4 Characterization of Pickering emulsions with 0.1% CNFs under different storage temperatures and pH values. (A and B) Images and emulsion index. (C) Optical microscopy images. (D) Particle size distribution. CNFs from HPH-10t of enzymatic residues in the *Osfc16* mutants and WT samples. ** represents significant difference between the mutant and WT samples using the Student's *t*-test at the $p < 0.01$ level ($n = 3$) with the increased percentage of the mutant relative to the WT, and the data are expressed as mean ± SD ($n = 3$).

stabilized with the optimal CNFs of enzymatic residues in both *Osfc16* and WT samples (Fig. 4A), we did not find out any alterations in EI values under largely varied storage temperatures (4 °C, 25 °C, and 50 °C) and pH values (pH = 3, pH = 5, and pH = 7) (Fig. 4B). In terms of the particle size distribution of Pickering emulsions, this study only observed slight alteration in the samples examined (Fig. 4C and D). Consistently, the Pickering emulsions of the *Osfc16* samples retained significantly increased EI values and reduced particle size distribution under different storage temperatures and pH values, except for the particle size distribution under pH = 7. Furthermore, during storage times from fresh to 24 days, the droplet sizes of Pickering emulsions were only reduced for the first 3 days in the WT samples, whereas the *Osfc16* samples did not show any altered droplet sizes (Fig. S3†). Therefore, the optimal CNFs generated in this study could well stabilize Pickering emulsions under different storage conditions, and particularly, the CNFs of enzymatic residues of *Osfc16* mutants could further improve Pickering emulsions' stability.

3.5. Enhanced biomass enzymatic saccharification and ethanol production in *Osfc16* mutants

As described above, despite that the residues obtained from direct enzymatic hydrolysis of raw straws required much less HPH cycle times for optimal CNFs than those of the raw straws, this study has also found out that the optimal CNFs of *Osfc16* mutant could better stabilize Pickering emulsions than the WT. Hence, we detected hexose yields from direct enzymatic hydrolysis of raw straws in both *Osfc16* mutant and WT (Fig. 5). By comparison, the *Osfc16* mutant exhibited significantly higher hexose yields than that of the WT at $p < 0.01$ level ($n = 3$) with the increased rate of 37% (Fig. 5A), which was consistent with the previous reports about remarkably enhanced biomass enzymatic saccharification in the *Osfc16* mutant under different chemical pretreatments.[33] Consequently, in this study, we performed classic yeast fermentation with hexoses and detected significantly increased bioethanol yields at $p < 0.01$ level ($n = 3$) by 19% in the *Osfc16* mutant (Fig. 5B). Therefore, the results indicated that the enzymatic residues of *Osfc16* mutants could not only generate the desirable CNFs for much improved Pickering emulsions, but also lead to additional higher bioethanol products.

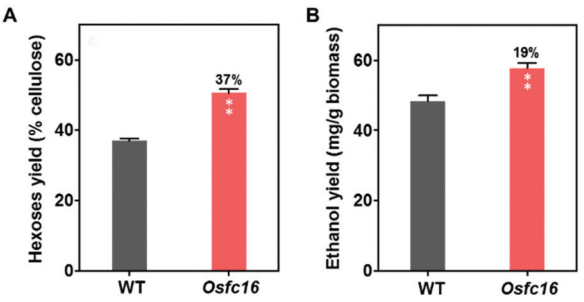

Fig. 5 Hexose and bioethanol yields achieved from the *Osfc16* and WT samples. (A) Hexose yields released from the direct enzymatic hydrolysis of raw rice straws. (B) Ethanol yields obtained by yeast fermentation with hexoses. ** represents significant difference between the mutant and WT samples using the Student's *t*-test at the $p < 0.01$ level ($n = 3$) with the increased percentage of the mutant relative to the WT, and the data are expressed as mean ± SD ($n = 3$).

3.6. Remarkably increased cellulase secretion from CNF co-incubation with *T. reesei* in *Osfc16* samples

Provided that the lignocellulose substrates could distinctively induce *T. reesei* strains to secret lignocellulose-degradation enzymes including cellulases and xylanases,[41,53] little has been yet reported about CNF induction role. In this study, we initially combined the raw straw substrate with different dosages of optimal CNFs of *Osfc16* mutants to incubate with *T. reesei* strains for cellulase and xylanase production (Fig. 6). Using our previously established approaches,[41] we determined filter paper activities (FPA) and total protein levels of those enzymes secreted by *T. reesei* (Fig. 6A–C). Compared with the control without CNF co-supply, all four samples co-supplied with different dosages of CNFs showed significantly increased FPAs and total protein contents up to 2 folds at $p < 0.01$ levels ($n = 3$). However, even though supplied with different dosages of CNFs, those four samples did not show any significantly different FPAs and protein levels, suggesting that the CNF co-supply should mainly act as an inducer, rather than as major carbon source for *T. reesei* secreting enzymes. Furthermore, this study co-supplied the optimal CNFs with two rice straws of the *Osfc16* mutant and WT to incubate with the *T. reesei* strain, respectively (Fig. 6D–H). As a result, both the *Osfc16* mutant and WT samples were of significantly increased FPAs by 1.3 and 1.6 folds from the CNF co-supplements (Fig. 6D). However, the sample of CNFs only (without raw rice straws) had extremely low FPA, which was even much lower than those of two raw straws only (without CNFs). Hence, this confirmed the assumption that the CNF co-supply may mainly play an inducing role for enzyme secretion by the *T. reesei* strain. Notably, even though co-supplied with the same amounts of CNFs, the *Osfc16* mutant samples remained higher FPAs than those of the WT, probably due to its reduced lignocellulose recalcitrance for effective carbon consumption by the *T. reesei* strain.[41,54–56]

With respect to the increased FPAs from the CNFs co-supplied with raw rice straws of the *Osfc16* mutant and WT, we further determined individual enzyme activity *in vitro* by incubating with total solutions secreted by *T. reesei* strains (Fig. 6E–H). Using pNPC, CMC-Na, salicin and beechwood xylan as standard substrates, this study detected relatively increased enzymatic activities including CBHI, EGII, BG and xylanases. In particular, both the *Osfc16* mutant and WT samples were of significantly increased activities of EGII and xylanases at $p < 0.01$ levels from the CNF co-supplements. In addition, this work performed LC-MS/MS analyses of *T. reesei*-secreted enzymes induced by combined *Osfc16* raw straws with its optimal CNFs (Table 1; Fig. S4 and S5†). This detected at least two cellobiohydrolases, four *endo*-β-1,4-glucanases, two β-glucosidases and two *endo*-1,4-β-xylanases, consistent with the previous findings that *T. reesei* could secret cellulase and xylanase complexes for complete lignocellulose degradation.[57]

3.7. Distinctively altered lignocellulose crystallinity and interlinkages from CNF co-incubation with *T. reesei* in the *Osfc16* samples

As the CNFs co-supplement with raw rice straws could induce *T. reesei* strain to secret relatively increased cellulases and xyla-

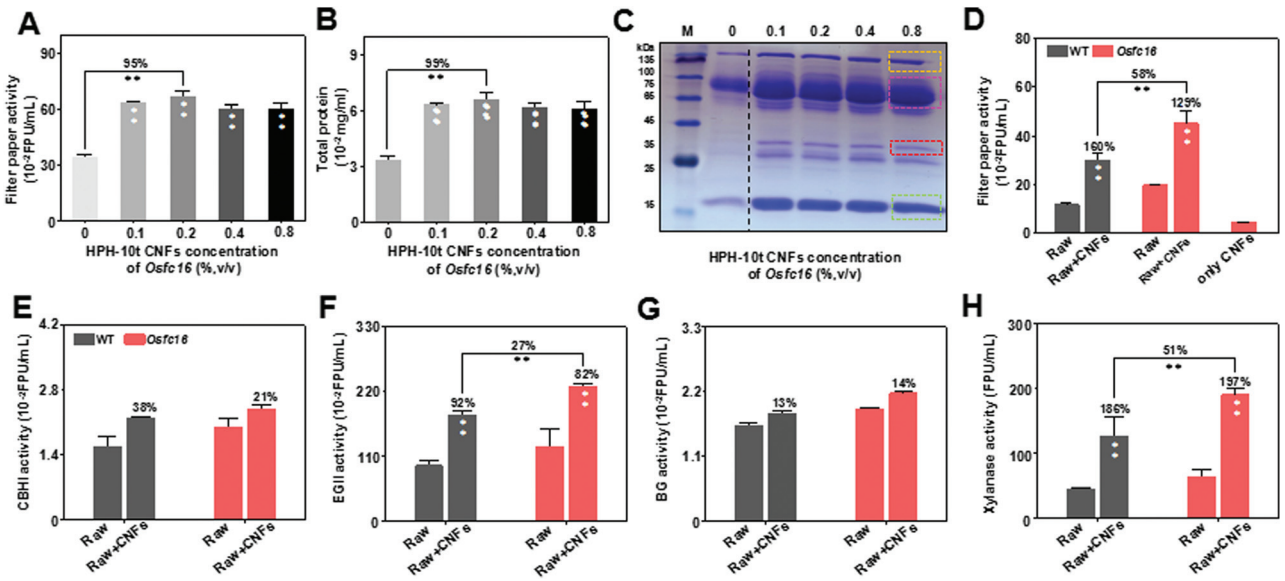

Fig. 6 Characterization of the cellulases and xylanases secreted by the *T. reesei* strain after incubation with raw rice straw co-supplied with CNFs. (A) Filter paper activity of enzymes secreted under different dosages of CNF co-supplements. (B) Total protein content; orange box highlighted for BG, pink for CBHI, red for EGII and green for xylanases. (C) SDS-PAGE images. (D) Comparison of the filter paper activity of the *Osfc16* mutant and WT co-supplemented with CNFs of HPH-10t of the enzymatic residue in rice mutants. (E–H) CBHI, EGII, BG and xylanase activity assay *in vitro*. ** represents significant difference between the two samples using the Student's *t*-test at the $p < 0.01$ level ($n = 3$) with the increased percentage, and the data are expressed as mean ± SD ($n = 3$).

Table 1 LC-MS/MS analyses of *T. reesei*-secreted enzymes incubated with *Osfc16* raw straw co-supplied with 0.2% CNFs from HPH-10t of the enzymatic residues of the *Osfc16* mutant

Protein name	Accession no.	iBAQ ($\times 10^6$)	MW [kDa]
Cellobiohydrolase I	A0A024RXP8	6.06	54.11
Cellobiohydrolase II	A0A024SH76	62.15	49.65
endo-β-1,4-Glucanase I	A0A024SNB7	145.11	48.21
endo-β-1,4-Glucanase II	A0A024SH20	4.67	44.15
endo-β-1,4-Glucanase IV	ETS06300	53.45	35.51
endo-β-1,4-Glucanase VII	A0A024SFJ2	422.64	26.8
endo-1,3-α-Glucosidase	A0A024SDT8	2.18	46.56
β-Glucosidase I	A0A024SB94	1.22	84.68
β-Glucosidase II	A0A024SD46	3.31	93.65
endo-1,4-β-Xylanase I	P36218	58.62	24.58
endo-1,4-β-Xylanase II	P36217	1745.9	24.07

nases, we examined the crystallinity and interlinkages of lignocellulose residues after *T. reesei* induction (Fig. 7). Compared to the raw rice straws, two remaining lignocellulose residue samples after incubation with *T. reesei* strain were of much increased cellulose crystalline index (CrI) values by 55% and 36%, respectively (Fig. 7A), which should explain that the non-crystalline cellulose and partial hemicellulose should be digested as a carbon source for *T. reesei* consumption.[58] Using our previously established approach,[44] this study detected all potential lignocellulose linkages of lignocellulose residues by FT-IR scanning (Fig. 7B; Table S2†). From the FT-IR spectra, seven peaks were altered in two residual samples relative to the raw straw samples, which were assigned as C–H, C–O–C and $C–H_2$ groups for cellulose association, and other groups such as C–H, C–O–C and –C═O for non-cellulosic polymer (lignin, hemicellulose, and pectin) interlinking.[6,59–64] In addition, we observed the alteration of the adsorption peak at 1368 cm^{-1} assigned as $C–H_2$ scissoring of cellulose between two residual samples, suggesting that the CNF co-supplement should play a role for effective cellulose digestion as a carbon source for *T. reesei* consumption.[62]

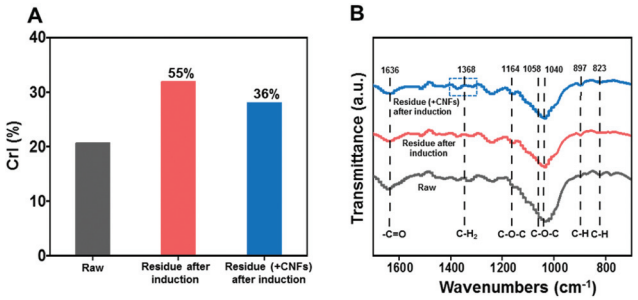

Fig. 7 Characterization of the lignocellulose residues after *T. reesei* incubation with *Osfc16* raw straws co-supplied with 0.2% CNFs obtained from HPH-10t of the enzymatic residues of the *Osfc16* mutants. (A) CrI of the lignocellulose residues. (B) FT-IR profiling of the lignocellulose residues, and all dot-lines indicate changed peaks as annotated in Table S2.† The percentages are expressed as increased CrI values in two residue samples relative to the raw control sample (without *T. reesei* incubation).

3.8. Characteristic CNF morphogenesis and features in *Osfc16* samples

To understand how the optimal CNF of *Osfc16* mutants could better stabilize Pickering emulsions or induce more *T. reesei* secretion of cellulases and xylanases as described above, this study applied AFM to observe CNF morphogenesis generated from either the raw rice straws or the enzymatic residues in both *Osfc16* mutants and WT (Fig. 8A). Despite that all four samples exhibited the CNFs at similar shapes, we observed the rough surfaces of CNFs consisting of defects with different distances to evaluate the average of nanofibril length (Fig. 8B).[65] By randomly selecting 50 CNF fragments, we calculated the average distances (nm) of two defects in the CNF samples. As a comparison, two residue samples of *Osfc16* mutant and WT respectively showed the average distances of defects on the CNF surfaces at 131.7 nm and 194.2 nm, whereas their raw rice straw samples had the average defect distances of 149.0 nm and 335.6 nm, indicating that the CNF surfaces of

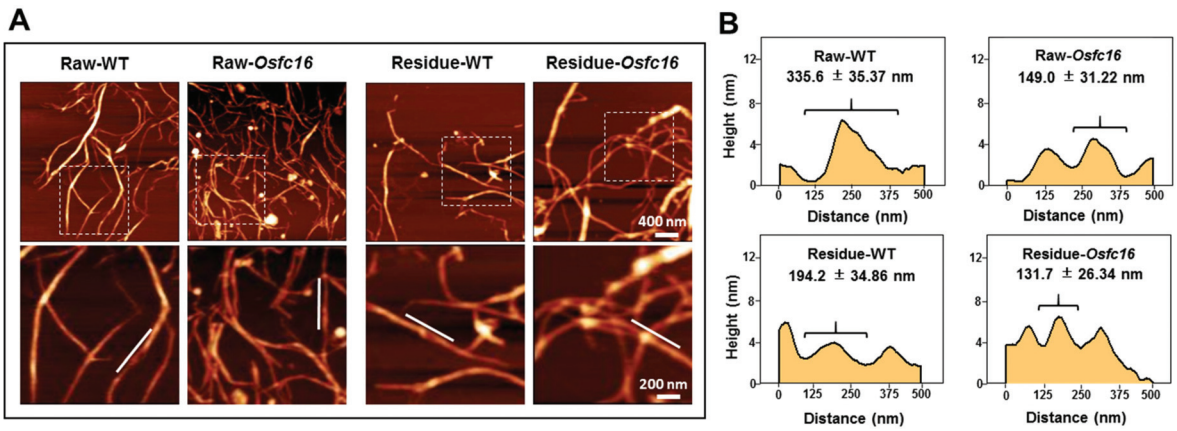

Fig. 8 Characterization of CNF morphogenesis from HPH-10t of raw straws and HPH-20t of enzymatic residues in the *Osfc16* mutants and WT. (A) AFM general images of the CNFs. (B) Evaluation of the average distance between two defects on the surfaces of the CNFs as highlighted in (A) to present the nanofibril length; the data are expressed as mean ± SD (n = 50).

the enzymatic residues contained much more defects than those of the raw rice straws. Meanwhile, it also indicated that the CNF surfaces of the *Osfc16* mutant were of more defects than those of the WT in both raw rice straw and enzymatic residue samples, suggesting that the *Osfc16* mutant could produce relatively short-length nanofibrils. Therefore, we assumed that the defects of CNFs should be the initial places enabled for *T. reesei* attachment and enzyme loading effective for cellulose degradation. However, these defects should be particularly favorable for interaction with organic chemicals to broadly stabilize the Pickering emulsions examined in this study.

3.9. Comparison of major biomass-process parameters with the previous findings

Based on all data obtained in this study, we presented comparisons with previous findings to highlight the major parameters improved for complete and multiple lignocellulose utilization of crop straws. In terms of improved Pickering emulsions, the generation of cellulose nanofibrils from *Osfc16* straws required less cycle times of homogenization by 2–4 folds, compared to the previous reports on *Miscanthus* and bacterial nanofibrils (Table 2). Even though under much less homogenization cycle times, the generated *Osfc16* nanofibrils could more upgrade major parameters of Pickering emulsions such as higher emulsion index and lower zeta potential and droplet size, as a comparison with other five distinct substrates including *Miscanthus* and bacterial nanofibrils, soy and wheat proteins and corn starch.[15,50,66–68] Because the desirable cellulose nanofibrils were obtained from direct enzymatic hydrolysis of raw rice straws, this study could meanwhile produce additional bioethanol, which should be of unique advantage among all previously established technologies. In addition, this study compared hexose yields (% cellulose) obtained from direct enzymatic hydrolysis of various crop raw straws, and the rice *Osfc16* mutant was of much higher hexose yield by 1.5–5 folds than those of other major crop straws reported in previous studies (Table 3), mainly due to remarkably low lignocellulose recalcitrance examined in the mutant, as described above.

Although little has been reported yet about the cellulose nanofibrils as inducers for enhancing *T. reesei* to secret lignocellulose-degradation enzymes, this study compared them with other chemical compounds supplied with *T. reesei*, as reported previously (Table 4). The FPA and total protein levels detected from *Osfc16* nanofibril induction were much more increased than those of other chemicals in particular for the xylanase activity.[32,69–71] However, the *Osfc16* nanofibril induction led to less increased CBHI activity compared to the chemical (NH_4OH, Mn^{2+}) supply.[32,70] Altogether, this study demonstrated three non-chemical biomass processes as the green-like technology for multiple and complete lignocellulose utilization such as initial direct enzymatic hydrolysis for additional bioethanol, sequential homogenization for desirable cellulose nanofibrils and final nanofibril induction for cellulase production.

Table 3 Comparison of hexose yields obtained from the direct enzymatic hydrolysis of crop raw straws in this study and in previous works

Material	Hexose yield (% cellulose)	Ref.
Rice (*Osfc16*)	**51**	**This study**
Wheat	20	7
Corn	33	10
Sugarcane	17	40
Miscanthus	10	42
Rapeseed	19	72
Sorghum	21	73

3.10. Mechanism of the desirable *Osfc16* mutant that was of multiple improvements

Regarding all novel findings achieved in this study, we proposed a mechanism model to explain why the *Osfc16* mutant was of multiple enhancements of Pickering emulsions, cellulase secretion and bioethanol production (Fig. 9). Because the *Osfc16* mutant has been characterized with significantly reduced lignocellulose-recalcitrance such as cellulose CrI and DP values,[21] this study determined much increased hexose yield from direct enzymatic hydrolysis of raw rice straws, leading to remarkably higher bioethanol yield in the mutant relative to its WT. Due to the direct enzymatic hydrolysis, the remaining residues of *Osfc16* mutants enabled the generation of the optimal CNFs under much less cycles of high-pressure homogenization, compared to its raw straws or ones of the WT. Notably, the CNFs of *Osfc16* mutants contained significantly more defects on their surfaces, which should not only be the initial places for attaching *T. reesei* to secret cellulases and xylanases at high protein yields and enzymes activities, but may also aid to load its secreted enzymes for activating

Table 2 Comparison of major Pickering emulsion parameters improved in this study and from previous reports

Material	Homogenization time	Emulsion index (%)	Zeta potential (mV)	Droplet size (μm)	Ethanol yield (mg g^{-1} biomass)	Ref.
***Osfc16* CNFs (raw)**	**20**	**65**	**−19**	—	—	**This study**
***Osfc16* CNFs (residue)**	**10**	**68**	**−19**	**7**	**58**	
Miscanthus CNFs	20	52	−15	18	—	15
Bacterial CNFs	40	62	−9	13	—	50
Soy protein	—[a]	51	—	43	—	66
Wheat protein	—	53	−4	92	—	67
Corn starch	—	—	−13	210	—	68

[a] Data not available or not detectable.

Table 4 Comparison of *T. reesei*-secreted biomass-degradation enzymes induced by cellulose nanofibrils in this study and by chemicals

Inducing substrate	FPA (%)	Total protein (%)	CBHI activity (%)	EGII activity (%)	BG activity (%)	Xylanase activity (%)	Ref.
***Osfc16* CNFs**	**129**[a]	**99**	**21**	**82**	**14**	**197**	**This study**
NH_4OH	—[b]	—	50	17	—	12	32
Furfural	13	17	—	87	—	—	69
Mn^{2+}	—	26	94	62	—	—	70
Rapamycin	22	35	20	15	—	—	71

[a] Increased rates of protein levels and enzymatic activities by inducing substrate compared to the control (without inducing substrate). [b] Data not detectable.

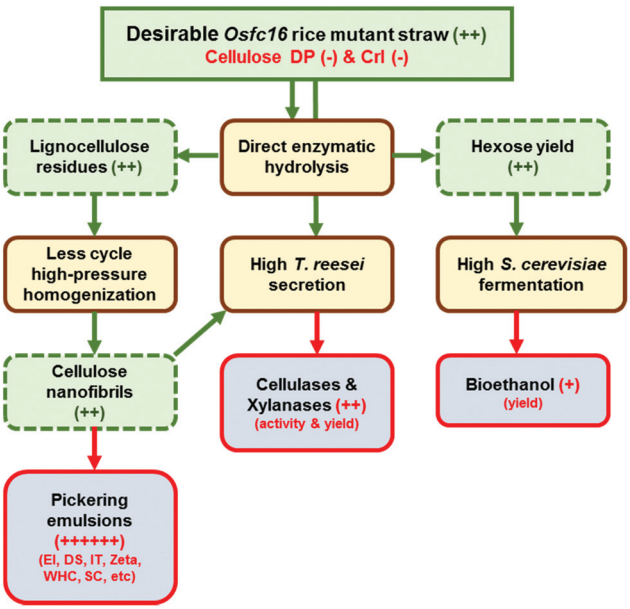

Fig. 9 A mechanistic model to elucidate distinct CNFs as stabilizers and inducers for improved Pickering emulsions and cellulase secretion coupled with bioethanol production in *Osfc16* relative to WT. (+) and (–) highlighted the increased and reduced features/parameters/factors. EI, emulsion index; DS, droplet size; IT, interfacial tension; Zeta, zeta potential; WHC, water holding capacity; SC, storage condition.

cellulose degradation as carbon source for consequent *T. reesei* induction. Meanwhile, such increased defects of the *Osfc16* mutant should be particularly favorable for the interaction between the CNFs and organic chemicals for broadly improved Pickering emulsions including almost all major parameters examined in this study. Hence, this model has highlighted that the optimal CNFs generated from the *Osfc16* mutant could act as an effective stabilizer and efficient inducer for improved Pickering emulsions and cellulase secretion coupled with high bioethanol production.

4. Conclusions

Using the desirable *Osfc16* mutant that is of recalcitrance-reduced lignocellulose, this study examined significantly increased hexose yield from direct enzymatic hydrolysis of raw straws towards higher bioethanol production. The remaining enzymatic lignocellulose residues were then required for much less cycle times of high-pressure homogenization to generate optimal CNFs that are of significantly more defects on the surfaces, which could act as inducers for *T. reesei* secretion of cellulases and xylanases in high yields and activity or as the stabilizer for extensive improvements of Pickering emulsions. Therefore, this study has demonstrated multiple roles of the CNF generated from recalcitrance-reduced lignocellulose residues, providing a green-like technology for cost-effective bioethanol and high-value bioproducts from full biomass utilization.

Conflicts of interest

The authors have no conflicts of interest to declare.

Acknowledgements

This work was in part supported by the National Science Foundation of China (32101701, 32170268), the Huazhong Agricultural University Independent Scientific & Technological Innovation Foundation (2662020ZKPY013; 2662019PY054), the National 111 Project of Ministry of Education of China (BP0820035), and the Project of Hubei University of Arts & Science (XKQ2018006).

References

1 P. Volkmar and S. Mats, *Renewable Sustainable Energy Rev.*, 2019, **103**, 5105–5116.
2 E. M. Rubin, *Nature*, 2008, **454**, 841–845.
3 Y. Li, P. Liu, J. Huang, R. Zhang, Z. Hu, S. Feng, Y. Wang, L. Wang, T. Xia and L. Peng, *Green Chem.*, 2018, **20**, 2047–2056.
4 D. W. Wakerley, M. F. Kuehnel, K. L. Orchard, K. H. Ly, T. E. Rosser and E. Reisner, *Nat. Energy*, 2017, **2**, 17021.
5 L. Peng, C. H. Hocart, J. W. Redmond and R. E. Williamson, *Planta*, 2000, **211**, 406–414.
6 Y. Wang, C. Fan, H. Hu, Y. Li, D. Sun, Y. Wang and L. Peng, *Biotechnol. Adv.*, 2016, **34**, 997–1017.
7 L. Cheng, L. Wang, L. Wei, Y. Wu, A. Alam, C. Xu, Y. Wang, Y. Tu, L. Peng and T. Xia, *Green Chem.*, 2019, **21**, 3693–3700.

8 H. Gao, Y. Wang, Q. Yang, H. Peng, Y. Li, D. Zhan, H. Wei, H. Lu, M. Bakr, M. EI-Sheekh, Z. Qi, L. Peng and X. Lin, *Renewable Energy*, 2021, **175**, 1069–1079.
9 M. Madadi, Y. Wang, C. Xu, P. Liu, Y. Wang, T. Xia, Y. Tu, X. Lin, B. Song, X. Yang, W. Zhu, D. Duanmu, S. Tang and L. Peng, *J. Hazard. Mater.*, 2021, **406**, 124727.
10 L. Wu, S. Feng, J. Deng, B. Yu, Y. Wang, B. He, H. Peng, Q. Li, R. Hu and L. Peng, *Green Chem.*, 2019, **21**, 4388.
11 S. A. Kedzior, V. A. Gabriel, M. A. Dubé and E. D. Cranston, *Adv. Mater.*, 2021, **33**, 2002404.
12 M. Kargar, K. Fayazmanesh, M. Alavi, F. Spyropoulos and I. Norton, *J. Colloid Interface Sci.*, 2012, **366**, 209–215.
13 T. Pettersson, J. Hellwig, P. Gustafsson and S. Stenström, *Cellulose*, 2017, **24**, 4139–4149.
14 L. Bai, S. Huan, W. Xiang and O. J. Rojas, *Green Chem.*, 2018, **20**, 15711582.
15 Q. Li, B. Xie, Y. Wang, Y. Wang, L. Peng, Y. Li, B. Li and S. Liu, *Food Hydrocolloids*, 2019, **97**, 105214.
16 H. Dua, C. Liu, Y. Zhang, G. Yu, C. Si and B. Li, *Ind. Crops Prod.*, 2016, **94**, 736–745.
17 F. Hu, J. Zeng, Z. Cheng, X. Wang, B. Wang, Z. Zeng and K. Chen, *Carbohydr. Polym.*, 2021, **254**, 117474.
18 R. Baati, A. Mabrouk, A. Magnin and S. Boufi, *Carbohydr. Polym.*, 2018, **195**, 321–328.
19 X. Zhang, Y. Li, X. Zhao and F. Bai, *Bioresour. Technol.*, 2017, **223**, 317–322.
20 T. Yang, Y. Guo, N. Gao, X. Li and J. Zhao, *Carbohydr. Polym.*, 2020, **234**, 115862–115869.
21 B. Sipos, Z. Benko, D. Dienes, K. Reczey, L. Viikari and M. Siika-aho, *Appl. Biochem. Biotechnol.*, 2010, **161**, 347–364.
22 R. Brunecky, V. Subramanian, J. Yarbrough, B. Donohoe, T. Vinzant, T. Vanderwall, B. Knott, Y. Chaudhari, Y. Bomble, M. Himmela and S. Decker, *Green Chem.*, 2020, **22**, 478.
23 Alokika and B. Singh, *Appl. Microbiol. Biotechnol.*, 2019, **103**, 8763–8784.
24 Y. Li, X. Zhang, L. Xiong, M. A. Mehmood, X. Zhao and F. Bai, *Bioresour. Technol.*, 2017, **238**, 643–649.
25 R. Singhania, H. Ruiz, M. Awasthi, C. Dong, C. Chen and A. Patel, *Renewable Sustainable Energy Rev.*, 2021, **151**, 111622.
26 C. Huang, X. Jiang, X. Shen, J. Hu, W. Tang, X. Wu, A. Ragauskas, H. Jameel, X. Meng and Q. Yong, *Renewable Sustainable Energy Rev.*, 2022, **154**, 111822.
27 Y. Wang, P. Liu, G. Zhang, Q. Yang, J. Lu, T. Xia, L. Peng and Y. Wang, *Renewable Sustainable Energy Rev.*, 2021, **137**, 110586.
28 D. Gomes, S. Serna-Loaiza, C. Cardona, M. Gama and L. Domingues, *Bioresour. Technol.*, 2018, **267**, 347–355.
29 A. Claesa, Q. Deparis, M. Foulquié-Moreno and J. Thevelein, *Metab. Eng.*, 2020, **59**, 131–141.
30 A. Petersen, O. Okoro, F. Chireshe, T. Moonsamy and J. Gorgens, *Energy Convers. Manage.*, 2021, **243**, 114398.
31 V. K. Gupta, A. S. Steindorff, R. G. Paula, R. Silva-Rocha, A. R. Mach-Aigner, R. L. Mach and R. N. Silva, *Trends Biotechnol.*, 2016, **34**, 970–982.
32 T. Kogo, Y. Yoshida, K. Koganei, H. Matsumoto, T. Watanabe, J. Ogihara and T. Kasumi, *Bioresour. Technol.*, 2017, **233**, 67–73.
33 F. Li, G. Xie, J. Huang, R. Zhang, Y. Li, M. Zhang, Y. Wang, A. Li, X. Li, T. Xia, C. Qu, F. Hu, A. J. Ragauskas and L. Peng, *Plant Biotechnol. J.*, 2017, **15**, 1093–1104.
34 D. Seibert-Ludwig, T. Hahn, T. Hirth and S. Zibek, *GCB Bioenergy*, 2019, **11**, 171–180.
35 Q. Li, Y. Wu, R. Fang, C. Lei, Y. Li, B. Li, Y. Pei, X. Luo and S. Liu, *Trends Food Sci. Technol.*, 2021, **110**, 573–583.
36 P. Paximada, E. Tsouko, N. Kopsahelis, A. A. Koutinas and I. Mandala, *Food Hydrocolloids*, 2016, **53**, 225–232.
37 O. Shezad, S. Khan, T. Khan and J. K. Park, *Carbohydr. Polym.*, 2010, **82**, 173–180.
38 J. Huang, Y. Li, Y. Wang, Y. Chen, M. Liu, Y. Wang, R. Zhang, S. Zhou, J. Li, Y. Tu, B. Hao, L. Peng and T. Xia, *Biotechnol. Biofuels*, 2017, **10**, 294.
39 Zahoor, Y. Tu, L. Wang, T. Xia, D. Sun, S. Zhou, Y. Wang, Y. Li, H. Zhang, T. Zhang, M. Madadi and L. Peng, *Bioresour. Technol.*, 2017, **243**, 319–326.
40 M. Hu, H. Yu, Y. Li, A. Li, Q. Cai, P. Liu, Y. Tu, Y. Wang, R. Hu, B. Hao, L. Peng and T. Xia, *Carbohydr. Polym.*, 2018, **202**, 434–443.
41 P. Liu, A. Li, Y. Wang, Q. Cai, H. Yu, Y. Li, H. Peng, Q. Li, Y. Wang, X. Wei, R. Zhang, Y. Tu, T. Xia and L. Peng, *Renewable Energy*, 2021, **174**, 799–809.
42 W. Jin, L. Chen, M. Hu, D. Sun, A. Li, Y. Li, Z. Hu, S. Zhou, Y. Tu, T. Xia, Y. Wang, G. Xie, Y. Li, B. Bai and L. Peng, *Appl. Energy*, 2016, **175**, 82–90.
43 W. Song, X. Han, Y. Qian, G. Liu, G. Yao, Y. Zhong and Y. Qu, *Biotechnol. Biofuels*, 2019, **9**, 68–82.
44 A. Alam, R. Zhang, P. Liu, J. Huang, Y. Wang, Z. Hu, M. Madadi, D. Sun, R. Hu, A. J. Ragauskas, Y. Tu and L. Peng, *Biotechnol. Biofuels*, 2019, **12**, 99–120.
45 D. Lin, R. Li, P. Lopez-Sanchez and Z. Li, *Food Hydrocolloids*, 2015, **44**, 435–442.
46 J. Xiao, Y. Li and Q. Huang, *Trends Food Sci. Technol.*, 2016, **55**, 48–60.
47 S. Fujisawa, E. Togawa and K. Kuroda, *Sci. Technol. Adv. Mater.*, 2017, **18**, 959–971.
48 C. C. Berton-Carabi and K. Schroën, *Annu. Rev. Food Sci. Technol.*, 2015, **6**, 263–297.
49 S. Shafiei-Sabet, M. Martinez and J. Olson, *Cellulose*, 2016, **23**, 2943–2953.
50 Q. Li, Y. Wang, Y. Wu, K. He, Y. Li, X. Luo, B. Li, C. Wang and S. Liu, *Food Hydrocolloids*, 2019, **88**, 180–189.
51 A. Pandey, M. Derakhshandeh, S. A. Kedzior, B. Pilapil, N. Shomrat and T. Segal-Peretz, *J. Colloid Interface Sci.*, 2018, **532**, 808–818.
52 H. Dai, J. Wu, H. Zhang, Y. Chen, L. Ma, H. Huang, Y. Huang and Y. Zhang, *Trends Food Sci. Technol.*, 2020, **102**, 16–29.
53 H. Fang, C. Zhao and X. Song, *Bioresour. Technol.*, 2010, **101**, 4111–4119.

54 D. Gao, N. Uppugundla, S. P. Chundawat, X. Yu, S. Hermanson, K. Gowda, P. Brumm, D. Mead, V. Balan and B. E. Dale, *Biotechnol. Biofuels*, 2011, **4**, 5–16.
55 V. Rana, A. D. Eckard, P. Teller and B. K. Ahring, *Bioresour. Technol.*, 2014, **154**, 282–289.
56 J. Deng, X. Zhu, P. Chen, B. He, S. Tang, W. Zhao, X. Li, R. Zhang, Z. Lv, H. Kang, L. Yu and L. Peng, *Sustainable Energy Fuels*, 2019, **4**, 607–618.
57 V. Novy, F. Nielsen, B. Seiboth and B. Nidetzky, *Biotechnol. Biofuels*, 2019, **12**, 238–254.
58 I. S. Druzhinina and C. P. Kubicek, *Microb. Biotechnol.*, 2017, **10**, 1485–1499.
59 H. C. Ong, W. Chen, Y. Singh, Y. Gan, C. Chen and P. L. Show, *Energy Convers. Manage.*, 2020, **209**, 112634.
60 Z. Cai, B. Ji, K. Yan and Q. Zhu, *Polymer*, 2019, **11**, 2071.
61 H. Guo, C. Hong, X. Chen, Y. Xu, Y. Liu, D. Jiang and B. Zheng, *PLoS One*, 2016, **11**, e0153475.
62 M. Balat, *Energy Convers. Manage.*, 2011, **52**, 858–875.
63 C. Xu, S. Hu, J. Xiang, L. Zhang, L. Sun, C. Shuai, Q. Chen, L. He and E. M. A. Edreis, *Bioresour. Technol.*, 2014, **154**, 313–321.
64 A. Baum, M. Dominiak, S. Vidal-Melgosa, W. G. T. Willats, K. M. Søndergaard, P. W. Hansen, A. S. Meyer and J. D. Mikkelsen, *Food Bioprocess Technol.*, 2016, **10**, 143–154.
65 M. Tyufekchiev, A. Kolodziejczak, P. Duan, M. Foston, K. Schmidt-Rohr and M. T. Timko, *Green Chem.*, 2019, **21**, 5541–5555.
66 H. Yang, Z. Su, X. Meng, X. Zhang, J. F. Kennedy and B. Liu, *Carbohydr. Polym.*, 2020, **247**, 116712.
67 M. Li, Z. He, G. Li, Q. Zeng, D. Su, J. Zhang, Q. Wang, Y. Yuan and S. He, *Food Hydrocolloids*, 2019, **90**, 482–489.
68 X. Lu, H. Liu and Q. Huang, *Food Hydrocolloids*, 2020, **103**, 105703.
69 C. Zhao, X. Liu, T. Zhan and J. He, *RSC Adv.*, 2018, **8**, 36233.
70 Y. Chen, Y. Shen, W. Wang and D. Wei, *Biotechnol. Biofuels*, 2018, **11**, 54.
71 A. Pang, H. Wang, F. Zhang, X. Hu, F. Wu, Z. Zhou, W. Wang, Z. Lu and F. Lin, *Biotechnol. Biofuels*, 2021, **14**, 77.
72 Y. Pei, Y. Li, Y. Zhang, C. Yu, T. Fu, J. Zou, Y. Tu, L. Peng and P. Chen, *Bioresour. Technol.*, 2016, **203**, 325–333.
73 F. Xu, J. Wang, M. Dong, S. Wang, G. Xiao, Q. Li, J. Chen, W. Li, W. Hu and J. Liu, *Carbohydr. Polym.*, 2019, **222**, 114976.